BIOCHEMISTRY
including biophysical chemistry & molecular biology

Article

pubs.acs.org/biochemistry

Isotropic Bicelles Stabilize the Juxtamembrane Region of the Influenza M2 Protein for Solution NMR Studies

Jolyon K. Claridge, Jussi Aittoniemi,[†] Daniel M. Cooper, and Jason R. Schnell*

Department of Biochemistry, University of Oxford, South Parks Road, Oxford, OX1 3QU, United Kingdom

Supporting Information

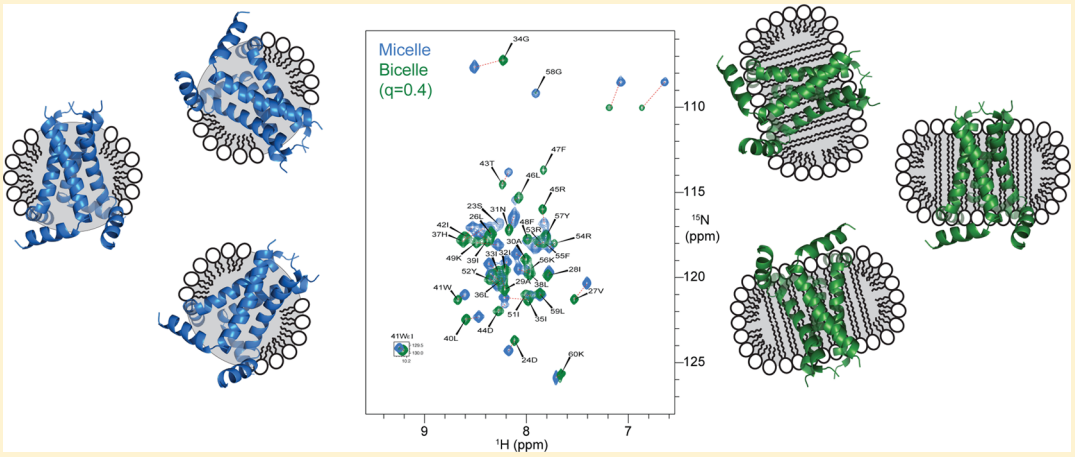

ABSTRACT: The protein M2 from influenza is a tetrameric membrane protein with several roles in the viral life cycle. The transmembrane helix (TMH) of M2 has proton channel activity that is required for unpackaging the viral genome. Additionally a C-terminal juxtamembrane region includes an amphipathic helix (APH) important for virus budding and scission. The APH interacts with membranes and is required for M2 localization to the site of viral budding. As a step toward obtaining high resolution information on the structure and lipid interactions of the M2 APH, we sought to develop a fast tumbling bicelle system, which would make studies of M2 in a membrane-like environment by solution NMR possible. Since M2 is highly sensitive to the solubilizing environment, an M2 construct containing the APH was studied under micelle and bicelle conditions while maintaining the same detergent and lipid headgroup chemistry to facilitate interpretation of the spectroscopic results. The sequence from a human H1N1 "swine flu" isolate was used to design an M2 construct (swM2) similar in amino acid sequence to currently circulating viruses. Comparison of swM2 solubilized in either the diacyl detergent 1,2-dihexanoyl-*sn*-glycero-3-phosphocholine (DHPC) or a mixture of DHPC and the lipid 1,2-dipalmitoyl-*sn*-glycero-3-phosphocholine (DPPC) (q = 0.4) indicated that the largest changes were a decrease in helicity at the N-terminus of the TMH and a decrease in dynamics for the juxtamembrane linker residues connecting the TMH and the APH. Whereas the linker region is very dynamic and the amide protons are rapidly exchanged with water protons in micelles, the dynamics and water exchange are largely suppressed in the presence of lipid. Chemical shift changes and relaxation measurements were consistent with an overall stabilization of the linker region, with only modest changes in conformation or environment of the APH itself. Such changes are consistent with differences observed in structures of M2 in lipid bilayers and detergent micelles, indicating that the bicelle system provides a more membrane-like environment.

The protein M2 from influenza is a type I membrane protein that forms a tetrameric proton-selective ion channel and has multiple roles in the viral life cycle.[1−3] The channel activity is required for unpackaging the viral genome as well as for preservation of the high-pH form of newly synthesized hemagglutinin as it is transported through the *trans*-Golgi network.[3−5] The transmembrane helix (TMH) is sufficient for channel activity and small molecule inhibition, which have been studied extensively (reviewed in refs 6−8).

Past circulating strains of M2 were sensitive to amino-adamantyl drugs, which inhibit proton channel activity. However, the past decade has seen a dramatic increase in resistance to the amino-adamantyls. The vast majority of the seasonal strains including the 2009 H1N1 "swine flu" pandemic and the 2013 H7N9 outbreak in China have asparagine at position 31, which confers drug resistance,[9−11] and the swine flu M2 is particularly insensitive to the amino-adamantyls.[12]

M2 has additional roles in the viral life cycle that are unrelated to the ion channel activity and may be targetable by

Received: July 31, 2013
Revised: October 29, 2013
Published: October 29, 2013

dx.doi.org/10.1021/bi401035m | *Biochemistry* 2013, 52, 8420−8429

antivirals. A membrane-interacting amphipathic helix (APH) that is C-terminal to the TMH is important for budding and scission,[13,14] while a second, more C-terminal region interacts with the matrix protein M1 for packaging of the viral ribonucleoprotein complex.[15,16] The APH of M2 (residues ~47−58) binds cholesterol and is proposed to target the protein to the edge of the host cell "budozone".[14,17−19] The isolated APH is sufficient for generating curvature in giant unilamellar vesicles,[13] and this activity may facilitate bud formation and scission of nascent virus particles.[19]

The conformation of M2 is sensitive to solubilizing conditions (reviewed in ref 20), indicating that changes in membrane structure induced by M2 and *vice versa* will be difficult to disentangle. Structural studies of M2 in detergents containing lipid-like head groups have been useful in studying to high resolution the TMH structure and drug interactions.[21−23] However, micelle curvature can distort the conformation of protein regions bound to the micelle surface (e.g., ref 24) and thus do not provide suitable systems for the study of juxtamembrane regions such as the APH of M2. Bicelles, however, formed from mixtures of lipid and detergent can form disk-like assemblies in which lipid bilayers form at the center and are surrounded by a ring of detergent molecules.[25−27] For mixtures of 1,2-dimyristoyl-*sn*-glycero-3-phosphocholine (DMPC) lipid and 1,2-dihexanoyl-*sn*-glycero-3-phosphocholine (DHPC) detergent at q values between ~0.25 and ~0.50, where q = [lipid]/[detergent], the bicelles tumble isotropically and at rates that permit recording of solution NMR data. Isotropic bicelles have been used in solution NMR studies to characterize small drug transporters,[28,29] transmembrane helix dimerization,[30−33] and the juxtamembrane domain of the epidermal growth factor receptor.[34] Thus, we sought to develop an isotropically tumbling bicelle system that stabilizes a native-like conformation of M2 to enable solution NMR studies of its interactions with membrane components.

To evaluate whether the addition of lipids provides a more membrane-like environment than detergent alone, a construct based on the 2009 H1N1 pandemic (swM2) was studied both in DHPC micelles and in mixtures of 1,2-dipalmitoyl-*sn*-glycero-3-phosphocholine (DPPC) and DHPC. Since the headgroups of DHPC and DPPC are identical and both contain two acyl chains, these compounds differ chemically only in the length of the acyl chains (6 and 16 carbon atoms, respectively). Structures of similar M2 constructs containing the TMH and APH have been determined in DHPC micelles[23] (PDB 2RLF) and in bilayers composed of 1,2-dioleoyl-*sn*-glycero-3-phosphocholine (DOPC) and 1,2-dioleoyl-*sn*-glycero-3-phosphoethanolamine (DOPE) lipids[35] (PDB 2L0J) providing a basis for evaluating differences in structure and dynamics due to the solubilizing environment (Figure 1). The overall Cα RMSD between the structures determined in micelles and membranes is 7 Å; however, this is reduced to only 1.65 Å across the TMH region. The major differences between the two structures are therefore in the APH and the linker residues connecting the TMH and the APH, which is likely due to different interactions in the headgroup regions of the detergent micelles and lipid bilayers.

In the spectroscopic comparison of swM2 in micelles and bicelles reported here, the largest changes in structure and dynamics upon addition of lipids were localized to the N-terminus of the TMH and the linker residues connecting the TMH and APH. These changes include a decrease in the flexibility and rates of chemical exchange with water in the TMH−APH linker region. Chemical shift changes indicated only a small increase in the stability of the APH, which was protected from water in both micelles and bicelles. Thus, it is concluded that bicelles stabilize the relative conformation of the TMH and APH and provide a more membrane-like environment for studies of M2−lipid interactions.

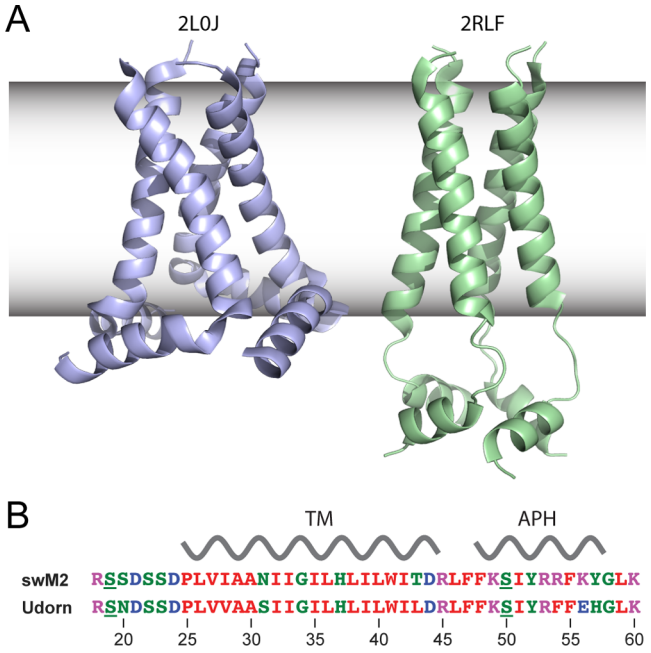

Figure 1. (A) Ribbon diagrams of Udorn M2 structures determined in membranes by solid state NMR (2L0J) and in DHPC micelles by solution NMR (2RLF). The presumed position of the membrane is shown in gray shading. (B) Amino acid sequence of the swM2 construct is shown aligned with that from Udorn. The underlined serine residues at positions 18 and 50 are substitutions for native cysteines.

MATERIALS AND METHODS

Plasmids. An *Escherichia coli* codon-optimized gene for the M2 protein associated with isolate A/New York/13/2009 H1N1 was purchased from GeneArt. The swM2 construct used for NMR studies contained residues 18−60, and a serine was substituted for the native cysteine at positions 19 and 50 (Supporting Information, Figure S1). Similarly to that of the Udorn variant,[23] the swM2 construct was subcloned into the pMMHb plasmid containing a trpLE fusion and an intervening methionine.

Protein Expression and Purification. Protein was expressed and purified similarly to the method described previously.[23,36] *E. coli* strain BL21 pLysS (Invitrogen) transformed with the appropriate expression plasmid was cultured aerobically at 37 °C in LB. When A_{600nm} reached 0.6, the cells were pelleted by centrifugation, washed with M9 medium, and pelleted and resuspended in 4-fold lower volume of M9 medium. After 20 min, appropriate isotopes were added. After a further 20 min, expression was induced with 1 mM final concentration of isopropyl β-D-1-thiogalactopyranoside, and the growth continued overnight before harvesting. The cells were resuspended in 50 mL lysis buffer (50 mM Tris-base, 150 mM NaCl, pH 8.0), sonicated, and then pelleted at 27 270g for 15 min. The supernatant was discarded, and the pellet resuspended in another 30 mL of lysis buffer and pelleted at

dx.doi.org/10.1021/bi401035m | *Biochemistry* 2013, 52, 8420−8429

27 270*g* for another 15 min. The resulting pellets were resuspended in guanidine buffer (6 M guanidine HCl, 50 mM Tris-base, 150 mM NaCl, pH 8.0) with the aid of a dounce homogenizer. The guanidine solution was then centrifuged at 18 000*g* for 90 min, and the supernatant was run over a Ni^{2+}-NTA-sepharose column, pre-equilibrated with guanidine buffer. The column was then washed with eight column volumes of guanidine buffer containing 20 mM imidazole. The fusion protein was eluted twice with two column volumes of guanidine buffer containing 400 mM imidazole. The eluate was dialyzed against 4 L of distilled water overnight, and the resulting precipitate was centrifuged at 500*g* for 30 min. The precipitate was then dissolved in 3 mL of formic acid. The fusion partner (trpLE) was cleaved by addition of 0.4 g of CNBr, and the reaction was allowed to proceed under a stream of nitrogen gas in darkness for 2 h. The reaction was then dialyzed against 4 L of distilled water for 1 h and freeze-dried. The dried protein was dissolved in HFIP/formic acid/water (2:1:2) and passed over a Zorbax 300 StableBond C3 HPLC column (Agilent) with a linear gradient from 10% to 100% buffer B (buffer A, 5% propan-2-ol, 0.1% TFA; buffer B, 58% propan-2-ol, 37% acetonitrile, 5% H_2O, 0.1% TFA). Fractions containing the protein were pooled and freeze-dried. The correct protein mass of the purified protein was verified by MALDI mass spectrometry.

NMR Sample Preparation. Micelle-solubilized samples of M2 were reconstituted into DHPC from 6 M guanidine as described previously.[23,36] Incorporation of the swM2 construct into lipid and detergent mixtures was attained by first forming lipid and protein thin films. Protein and lipid were dissolved in chloroform and methanol (3:1) and dried under a stream of nitrogen gas in 125 mm × 20 mm Pyrex round-bottom tubes (Corning). The film was then redissolved in neat chloroform and again dried under nitrogen. The thin films were dried under vacuum overnight to remove any remaining solvent and then rehydrated with NMR buffer (50 mM HEPES, 47 mM arginine, 30 mM glutamate, 0.05% azide, pH 7.2). Liposomes were formed by freeze−thaw cycles of the protein/lipid suspension with the thawing step carried out in a 42 °C water bath. DHPC was then added from a 500 mM stock solution. Lipids and detergent were purchased from Avanti Polar Lipids, Inc., in powder form and stored at −80 °C.

Chemical Cross-linking. Cross-linking was performed using glutaraldehyde. Aliquots of a 25% glutaraldehyde stock solution were added to NMR samples to a final glutaraldehyde concentration of 2 mM. Samples were incubated at 25 °C for 30 min, followed by quenching with 1 M Tris buffer (final concentration 200 mM), pH 8.0.

NMR Spectroscopy. All NMR spectra were collected at 30 °C unless otherwise indicated. Resonances of M2 in micelles and bicelles were assigned using 3D HNCA, 3D CBCACONH, 3D HNCO, and 3D HNCACO spectra at 500 MHz collected on triply labeled protein (^{15}N, ^{13}C, and ∼70% ^{2}H). Spectra were processed using NMRPipe[37] and analyzed using CARA[38] or CCPN analysis.[39] ^{15}N T_1 and T_2 experiments were carried out at 500 MHz using pulse sequences based on the method of ref 40; 1024 points were acquired in the direct dimension and 256 in the indirect. CLEANEX experiments were carried out at 500 MHz according to the method of ref 41, and errors were estimated from propagation of the spectral noise in each experiment using CCPN Analysis.

One-dimensional TRACT experiments[42] were recorded at 600 MHz (^{1}H) using 64 points collected at 2 ms intervals. Signal intensities were obtained by integrating over the ^{1}H spectral region from 8.2 to 8.8 ppm. The rotational correlation time (τ_m) was determined by fitting the differences in the relaxation due to the ^{15}N α- and β-spins according to eqs 3−6 of Lee et al.,[42] using the parameters $\theta = 17°$, $r_{HN} = 1.02$ Å, and $\Delta\delta_N = 160$ ppm.

Water-soluble paramagnetic relaxation enhancements were measured with SOFAST HMQCs at 500 MHz. Experiments consisting of 640 scans and 128 increments (total acquisition time 5 h) were recorded before and after addition of either 1 mM EDDA-Mn^{2+} or DTPA-Gd^{3+} from buffered stock solutions. The ratios of I/I_o and error estimations based on propagation of the spectral noise were calculated using CCPN analysis.

For measurement of residual dipolar couplings (RDCs), a ^{15}N labeled sample was partially aligned using a stretched gel.[23,43,44] The sample was soaked into a cylindrical polyacrylamide gel (6 mm in diameter) containing 4.4% (w/v) acrylamide at an acrylamide/bisacrylamide molar ratio of 37.5, and the set gel was squeezed into a 5 mm NMR tube (4.2 mm inner diameter) using the gel apparatus (New Era Enterprises). RDCs were measured at 750 MHz (^{1}H) and determined by subtracting the scalar coupling (J) measured on an unaligned sample from the measured coupling (J + RDC) of the aligned sample. $^{1}H-^{15}N$ couplings were determined from pairs of HSQC and TROSY spectra with 75 ms of ^{15}N evolution. The data were fit to dipolar waves[45,46] using the program QTI plot.

RESULTS

Swine M2 Oligomerizes under NMR Conditions. A construct based on an M2 sequence associated with the human "swine" influenza (H1N1) was designed for study (Figure 1B and Supporting Information, Figure S1). The swM2 construct differs from the Udorn strain by the following substitutions in the TM domain: V28I, S31N, and L40T. Amino acid differences in the APH include a substitution of tyrosine for histidine at position 58, which results in at least two overlapping cholesterol recognition motifs.[47] Other substitutions result in a larger positive charge of the swM2 APH than that of Udorn (+5 versus +3). With the exception of the C50S substitution, the swM2 APH sequence is also identical to that from a representative isolate of the 2013 outbreak of H7N9.[11]

The native oligomeric state of M2 in infected cells is tetrameric.[48,49] To test whether swM2 forms tetramers under NMR conditions, the protein was reconstituted into either DHPC micelles or DPPC/DHPC (q = 0.4) bicelles at NMR concentrations, chemically cross-linked, and analyzed by SDS-PAGE. In both micelles and bicelles, cross-linked swM2 exhibited a maximum band at approximately 28 kDa, indicating that swM2 is competent for oligomerization and that the oligomer stability was comparable with or without lipids (Supporting Information, Figure 2). The apparent molecular weight of the presumed tetramer was higher than anticipated for swM2 (28 kDa versus 20 kDa), although the observed oligomeric mass is approximately four times that of the uncross-linked monomer before taking into account any additional mass from the cross-linking reagent. In contrast, the apparent molecular weight of the major monomer species in the cross-linked sample had unusually high mobility compared with the monomer species in the uncross-linked sample. A similar result has been routinely observed in our laboratory for other single-pass transmembrane proteins containing a large

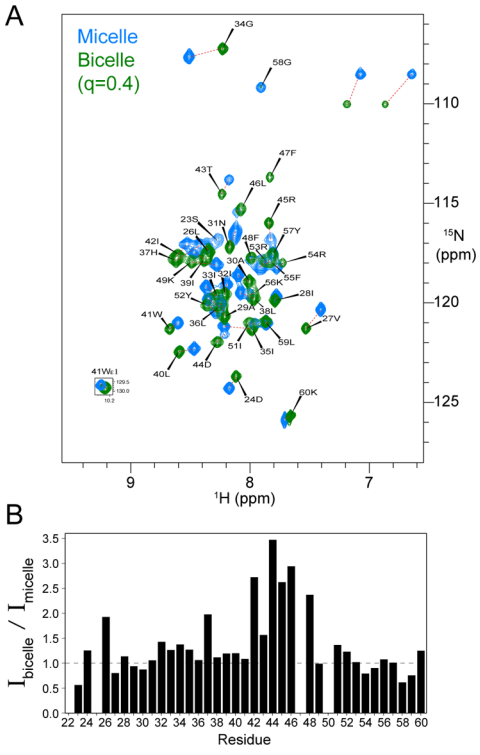

Figure 2. (A) Overlays of fast HSQC spectra of swM2 in DHPC micelles (blue) and DPPC/DHPC bicelles (q = 0.4) (green) at 30 °C, pH 7.2, at 500 MHz. The inset shows the peak corresponding to the HNε_1 of Trp41. Dashed red lines connect peaks in the two spectra corresponding to the same residue. (B) Relative ^{1}H,^{15}N crosspeak intensities for swM2 in DHPC micelles and DPPC/DHPC bicelles (q = 0.4) in fast HSQCs collected with identical experimental parameters for samples of similar protein concentration.

number of basic amino acids. The cause for the altered mobility of the cross-linked monomer and tetramer samples is not known, but anomalous mobility of membrane proteins on SDS gels is common.[50,51]

Low molecular weight bands corresponding approximately to the theoretical mass of swM2 (5038 Da) were detected in both cross-linked and uncross-linked samples. The presence of a monomeric band in addition to a tetrameric band after M2 cross-linking has been observed previously for an S31N variant of the Udorn strain of M2.[52] This result is consistent with a destabilizing effect of the S31N substitution. No peak doubling was observed in NMR spectra of swM2 in either micelle or bicelle conditions (see below) suggesting that the protein adopted a uniform oligomeric state on the NMR time scale.

Spectral Characterization of swM2. Both micelle and bicelle conditions provided high quality NMR spectra of swM2 (Figure 2A). Nearly complete chemical shift assignment was possible for backbone $^{1}H_N$, ^{15}N, $^{13}C\alpha$, and $^{13}C'$ and side chain $^{13}C\beta$ nuclei. However, several crosspeaks for residues in the linker region between the TMH and APH were comparatively weak in spectra of swM2 in DHPC micelles. A plot of the relative crosspeak intensities in micelles and bicelles indicated that the introduction of lipids resulted in a large increase in intensity for residues 42–48, which corresponds to the TMH C-terminus and the TMH–APH linker region (Figure 2B). Assignments for some of the weakest backbone amide ^{1}H and ^{15}N resonances (residues R45, L46, F47) were obtained by following the assigned bicelle resonances in a titration against DHPC, but several $^{13}C\alpha$ and $^{13}C'$ chemical shifts in the TMH–APH linker in micelles could not be assigned using triple resonance experiments.

For many resonances that could be observed both in micelles and bicelles, extensive chemical shift changes were observed between the two conditions (Figure 2A and 3) indicating that

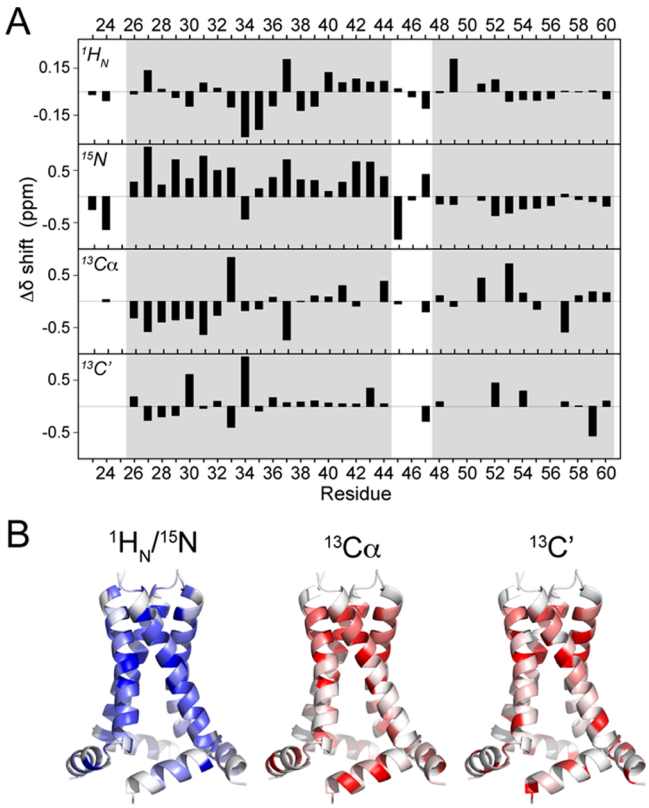

Figure 3. (A) Chemical shift differences ($\Delta\delta$) between swM2 in bicelles and micelles ($\Delta\delta$ = δ(bicelle) − δ (micelle)) plotted as a function of residue. Regions of the plot corresponding approximately to the TMH (residues 26–44) and APH (residues 48–60) are shaded. In panel B, the chemical shift differences between swM2 in bicelles and micelles ($\Delta\delta$) are mapped onto a homology model of swM2. The swM2 homology model was generated using the program SwissModel with 2L0J as a template.

the swM2 structure, environment, or both were influenced by the presence of lipid. In contrast, comparison of the backbone amide resonances in q = 0.3 and q = 0.4 bicelles indicated that the protein structure was not very sensitive to the q value in this range and that lipid-induced changes in structure decreased at higher q values (Supporting Information, Figure S3).

To confirm that swM2 interacted directly with lipids in bicelles, the ^{1}H–^{1}H plane of an ^{15}N-selected NOESY was recorded on a DPPC/DHPC bicelle sample in which the acyl chains of DPPC were protonated and the DHPC acyl chains were deuterated (Supporting Information, Figure S4). A large number of crosspeaks at the lipid methyl proton (~0.87 ppm) and methylene proton (~1.27 ppm) chemical shifts confirmed that the protein makes extensive contacts with lipids.

Chemical shift changes upon addition of DPPC were observed in the $^{13}C\alpha$ and $^{13}C'$ nuclei of residues Val27 to Ile32 at the N-terminus of the TMH. The majority of these changes were negative in bicelles, suggesting a slight decrease in helicity for this region in bicelles. Residues Ile33 and Gly34 at

dx.doi.org/10.1021/bi401035m | Biochemistry 2013, 52, 8420–8429

the center of the TMH exhibited the largest TMH changes in $^{13}C\alpha$ and $^{13}C'$, respectively. Large shift changes were also observed in the ^{15}N and $^{13}C\alpha$ of His37. In the TMH−APH linker, a relatively large backbone ^{15}N chemical shift change was observed for Arg45 and smaller changes in Phe47. Finally, smaller changes were observed in the $^{13}C\alpha$ shift of Ile51, Arg53, and Tyr57 and in the $^{13}C'$ shift of Tyr52, Arg54 and Leu59 in the APH.

Chemical shift analysis[53] was consistent with a helical conformation for residues ∼23−55 in both micelles and bicelles (Supporting Information, Figure S5A). However, the random coil index (RCI), which extracts an S^2 order parameter through a comparison of chemical shifts with random coil values,[53,54] indicated slightly decreased order at the C-terminal end of the APH for swM2 in micelles (Supporting Information, Figure S5B).

For comparison with the swM2 results, the Udorn strain M2 construct of the same length was tested also in micelles and bicelles (Supporting Information, Figure S6). Although a similar magnitude of chemical shift perturbations were observed upon addition of DPPC, the spectrum of the Udorn construct exhibited much lower spectral quality than that of swM2. To explore whether the higher spectral quality of swM2 was specific to DPPC, swM2 was reconstituted into lipids containing either DMPC, POPC/POPG (7:1), or DOPC/DOPE (4:1) (Supporting Information, Figure S7). Notably, all of the additional lipids tested have gel-transition temperatures well below the temperatures at which the spectra were recorded. Overlays of the HSQCs of these samples with that containing DPPC/DHPC bicelles indicated very similar chemical shifts. By contrast, the spectra of any one of the lipid mixtures overlaid poorly with that of swM2 in micelles. These results indicated that the protein adopted a similar conformation in all of the bicelle mixtures, and that none of the lipids tested made specific interactions with the protein.

Amide−Water Proton Exchange of swM2. The reduced cross-peak intensity observed for the linker residues in micelles may have arisen in part from rapid amide proton exchange with water. Therefore, the chemical exchange of the amide protons with water protons was measured using CLEANEX experiments.[41] The swM2 protein showed marked differences in proton exchange in the linker region residues L46 and F47 in micelles (Figure 4). In contrast, these residues exhibited low to moderate proton exchange in the bicelle sample, indicating that the structure of the linker region is more structured or more sequestered from water in the bicelle sample or both.

In both samples, the lowest amide−water proton exchange rates were observed in the TMH, with a small increase in exchange at Asn31 in both conditions. NOEs to water have previously been observed at this position (Ser31 in Udorn),[23,52] indicating that a water interaction is conserved at this site. Water exchange rates in the APH were similar in the two conditions, with increased exchange at Gly58 suggesting at least partial disruption of the APH at this position.

Comparison of Backbone Amide Dynamics. In order to explore differences in swM2 tumbling time and dynamics in micelles and bicelles, the backbone amide relaxation rates were measured (Figure 5A,B). The average ^{15}N R_1 and R_2 rates of 1.1 and 0.8 s^{-1} and 16.8 and 24.3 s^{-1} for residues 26−57 of swM2 in micelles and bicelles, respectively, resulted in average R_2/R_1 ratios of 16.2 and 29.8. From these R_2/R_1 values, estimates of the rotational correlation times[55] of 15.1 and 20.9 ns, respectively, were determined. TRACT experiments[42] were

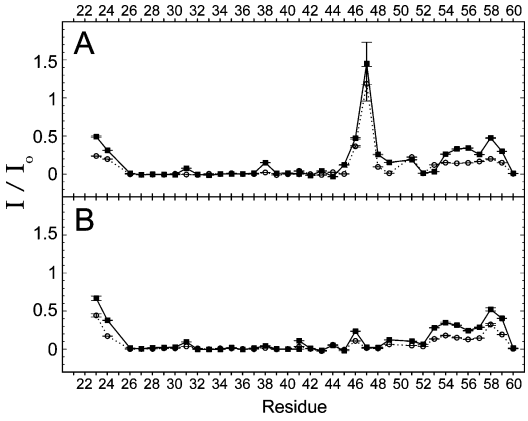

Figure 4. Backbone amide proton exchange with water using CLEANEX experiments in (A) micelles and (B) bicelles at 500 MHz. Water proton exchange is shown as the ratio of the $^1H/^{15}N$ crosspeak intensities in CLEANEX experiments with and without a 10 ms (open circles with dashed lines) or 30 ms (filled squares and continuous lines) mixing time. Exchange peaks for the Trp41 HNε1 are indicated with gray symbols.

also recorded to provide an independent estimation of the rotational correlation times. The resulting differences in relaxation rates for α and β components of the magnetization (25 and 36 Hz, for micelles and bicelles, respectively, at 600 Hz (^1H); Supporting Information, Figure S8) indicated rotational correlation times of 14.1 and 20.4 ns for swM2 in micelles and bicelles, respectively. These values were in good agreement with estimates from the R_2/R_1 values and consistent with a much larger protein−bicelle complex.

In the absence of structural information, plots of R_1R_2 versus R_2/R_1 can permit discrimination between intramolecular motions and rotational diffusion anisotropy.[56] While R_2/R_1 is sensitive to any motional anisotropy, the R_1R_2 values are largely independent of motional anisotropy. Plotting R_1R_2 versus R_2/R_1 for swM2 in micelles and bicelles highlights notable differences in protein motion between the two environments (Figure 5C,D). For swM2 in bicelles, the large standard deviation for R_2/R_1 values compared with that for R_1R_2 (8.3 s^{-1} versus 2.3 s^{-1}, respectively, for residues 26−57) indicated a large degree of motional anisotropy, as might be expected if the bicelle lipids were forming a disk-like bilayer. In contrast, the R_2/R_1 and R_1R_2 standard deviations for swM2 in micelles are more similar (5.7 s^{-1} and 4.7 s^{-1}, respectively, for residues 26−57), consistent with a spherical protein and micelle complex.

In both micelle and bicelle samples, the observable N-terminal residues Ser23 and Asp24, and the C-terminal residues Leu59 and Gly60 have R_1R_2 values much lower than the mean, indicating the presence of fast motions on the picosecond to nanosecond time scale. In micelles, the larger R_1R_2 of the APH residues 48−57 (19.8 s^{-2} versus 17.5 s^{-2} for the TMH residues) were indicative of exchange broadening (Figure 5C). In contrast, the R_1R_2 values of APH residues were similar to those of TMH residues in bicelles (19.7 s^{-2} versus 20.6 s^{-2} for the APH and TMH, respectively), indicating that the slow time scale motions were largely eliminated in bicelles (Figure 5D). The smaller standard deviation in R_1R_2 for swM2 TMH and APH residues (excluding the linker residues 45−47) in bicelles (2.0 s^{-2} versus 3.2 s^{-2} in micelles) indicated that internal protein dynamics in the presence of lipids are more homogeneous overall.

dx.doi.org/10.1021/bi401035m | Biochemistry 2013, 52, 8420−8429

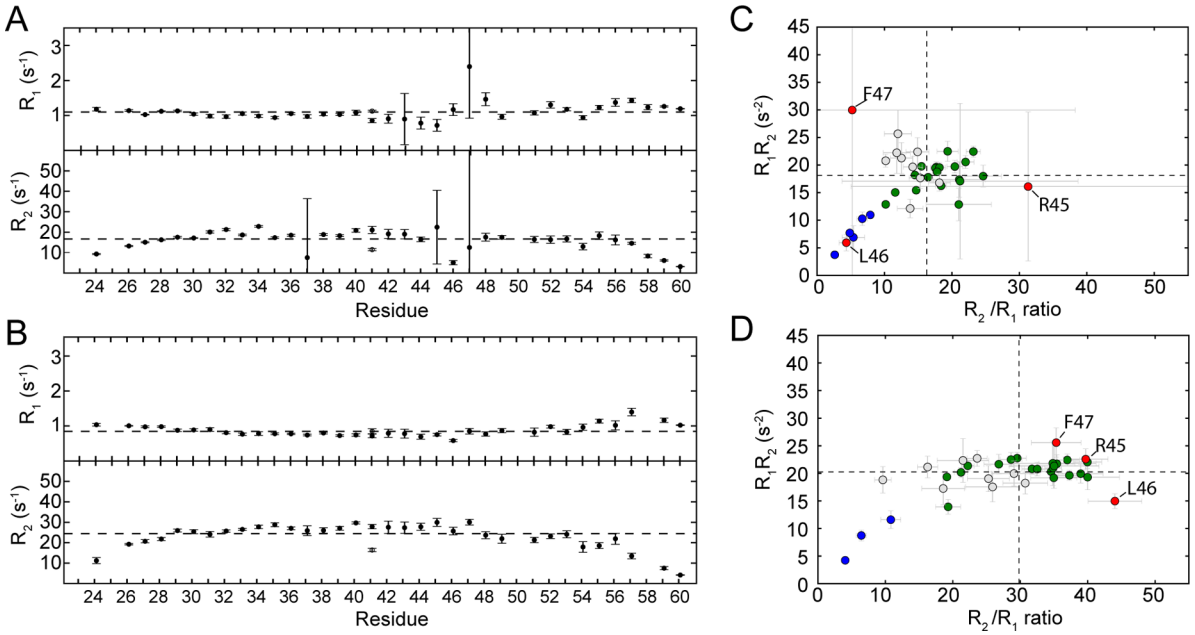

Figure 5. ^{15}N longitudinal (R_1) and transverse (R_2) relaxation rates of swM2 in (A) micelles and (B) bicelles at 500 MHz as a function of residue number. Plot of the ^{15}N R_1 and R_2 products versus the R_2/R_1 ratios for (C) micelles and (D) bicelles. In panels C and D, the position of the residues in the structure are indicated by the symbol color: blue for N- and C-termini residues, green for TMH residues, red for the TMH−APH linker region residues, and gray for APH residues. The data points for linker residues Arg45, Leu46, and Phe47 are labeled. In all plots, the dashed line indicates the 10% trimmed mean.

The APH Is Protected from Solvent in Both Micelles and Bicelles. Since most of the APH chemical shift changes between micelles and bicelles were smaller than the differences in the TMH (Figure 3A), it was investigated whether the APH has a similar degree of protection from solvent in micelles and bicelles. The water accessibility of the protein was probed using the water-soluble paramagnetic reagent EDDA-Mn^{2+}. The results show that the APH has a similar level of protection to the TMH in both conditions, being significantly more protected than the N- and C-termini (Figure 6). This indicated that the APH was embedded in micelles and bicelles to a comparable degree. Interestingly, however, the overall magnitude of the protection was lower for both the TMH and the APH in micelles. The difference in maximum protection in micelles versus bicelles was not due to a specific interaction of the EDDA-Mn^{2+} with DHPC, since experiments with a second water-soluble paramagnetic reagent, DTPA-Gd^{3+}, produced a similar result (data not shown).

The TMH Is Kinked at Gly34 in Both Micelles and Bicelles. Backbone amide ^{1}N−^{15}H residual dipolar couplings (RDCs) were measured for swM2 in DHPC micelles and DPPC/DHPC bicelles in order to probe for helix deformations and differences in helix angles (Figure 7). Attempts to soak the

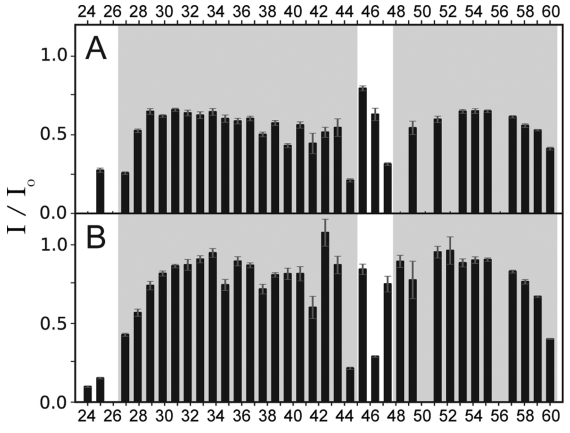

Figure 6. Water-soluble paramagnetic relaxation enhancement measurements for swM2 in (A) micelles and (B) DPPC bicelles at 500 MHz. The relaxation enhancement was taken to be inversely proportional to the intensity ratio measured after (I) and before (I_o) addition of 1 mM EDDA-Mn^{2+}.

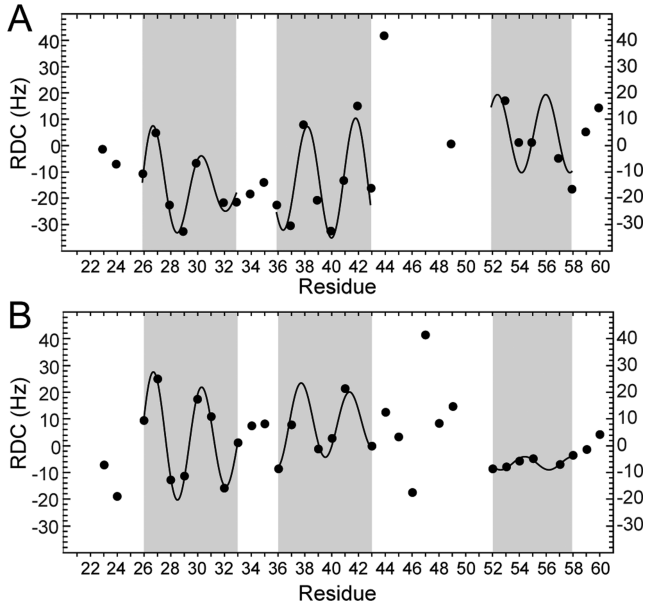

Figure 7. RDCs plotted against residue number for (A) micelles and (B) bicelles (q = 0.3), measured at 750 MHz. In both plots, separate dipolar waves were fit to residues 26−33, 36−43, and 52−58 (shaded).

dx.doi.org/10.1021/bi401035m | Biochemistry 2013, 52, 8420−8429

q = 0.4 bicelle sample into polyacrylamide gels for partial alignment failed. However, a sufficient concentration of q = 0.3 bicelles could be made to enter the gel matrix to enable accurate measurement of peak positions. Since only small changes were observed between spectra of swM2 at q = 0.3 and q = 0.4 (Supporting Information, Figure S3), RDC values were measured at the lower q value.

Dipolar waves could not be fit to the entire TMH satisfactorily in either micelles or q = 0.3 bicelles due to a discontinuity near Gly34. Thus, dipolar waves were fit to two segments of the TMH, residues 26−33 and 36−43. In micelles, the average amplitudes of the RDCs for the two segments of the TMH are similar (with average absolute amplitudes of 19.1 and 19.8 Hz), whereas in bicelles the discontinuity at Gly34 is accompanied by a change in amplitude of the dipolar wave (average absolute amplitudes 13.0 and 6.7 Hz). Changes in heavy atom chemical shifts in the N-terminal segment of the TMH (residues 26−31) and the kink residues Ile33 and Gly34 between the micelle and bicelle samples (Figure 3) indicated a probable change in kink angle. In addition, amide proton chemical shifts of Gly34 and Ile35 were moved upfield suggesting the possibility of increased hydrogen bonding in these amides.[57]

Dipolar waves were fit also to APH residues 52−58. A significant difference in the average magnitude of the RDC values for the APH in micelles and bicelles was observed. To test whether the swM2 conformation was more similar to the solid state or solution NMR structure in each condition, the swM2 RDCs that were fit to dipolar waves (Figure 7) were fit to the corresponding PDB structures (Table 1). The quality of the fit of the swM2 micelle RDCs was better for the solution NMR structure, but the fits of the swM2 bicelle data to the solution and solid state structure were more similar. More striking, the quality of the fits of the swM2 bicelle RDC data to either structure was 2−3-fold higher than that for the micelle RDC data.

Table 1. Quality of Fits of RDC Data to Structural Models[a]

swM2 RDC data	2L0J	2RLF
micelle	52.6	33.1
bicelle	17.2	14.5

[a] χ^2 values obtained for fitting backbone amide RDCs from residues 26−33, 36−43, and 52−58 to a single monomer from the indicated PDB structures.

DISCUSSION

The M2 protein from the influenza virus is involved in several stages of the viral life cycle. Although the ion channel activity of M2 required for unpackaging the viral genome and preserving the uncleaved conformation of hemagglutinin in the *trans*-Golgi network is well studied, the molecular basis for the role of M2 in viral budding remains poorly understood. The sensitivity of M2 structure to changes in the solubilizing environment, either between detergent micelles and lipid bilayers or between membranes with different lipid compositions (reviewed in ref 8), makes dissecting M2 structure and interactions challenging. We have evaluated here whether solubilization in bicelles provides a more membrane-like environment for studying M2 constructs containing both the TMH and the APH by solution NMR to enable high resolution studies of APH interactions with lipids.

In order to facilitate evaluation of bicelles as a membrane mimetic, the structure and dynamics of swM2 were studied in DHPC alone and in DHPC plus the lipid DPPC. Since DHPC and DPPC have identical headgroup chemistry and both contain saturated acyl chains, these studies permit a direct measure of protein conformational changes that arise from the different physical properties of the micelle and bicelle environments. Structures of M2 constructs containing the APH that have been determined previously in detergent[23] and lipid bilayers[35] provide a basis for rationalizing the differences observed for swM2 in micelles and bicelles. In the previously determined structure of Udorn in DHPC micelles, low signal-to-noise ratios for residues 47−51 precluded determination of the linker region conformation making it impossible to directly determine whether or how the APH packed against the TMH.[23] In contrast, the structure of a similar construct of Udorn M2 in oriented lipid bilayers that was determined using solid state NMR indicated that the APH is longer and that the TMH−APH linker is more ordered in membranes.[35]

The differences between swM2 in micelles and bicelles are consistent with the increased stabilization of the TMH−APH linker observed between the previously reported structures of M2 in micelles and lipid bilayers. The measurements made here indicated a high degree of disorder in the linker residues similar to that of the Udorn M2 construct in micelles. The addition of DPPC to form bicelles resulted in large spectral changes, the largest of which occurred in the TMH−APH linker region: large heavy atom chemical shift changes in Arg45 and Phe47, suppression of the large amide−water exchange rates of Leu46 and Phe47, and elimination of fast time-scale motions in Leu46.

The homogeneity of the swM2 bicelle spectra and the observation of extensive NOEs between protein and lipid indicated that the protein and lipids were well mixed. As expected, the addition of lipids to the protein complex resulted in increased rotational correlation time. However, the slower rotational correlation time of swM2 in bicelles did not result in a significant degradation of the spectral quality. Instead, it was found that the quality of the swM2 spectra in bicelles was superior to that in micelles. This was most striking for the linker region, but many signals in the APH also exhibited significantly worse spectral qualities in micelles. The poor spectral quality in the APH could be attributed to chemical shift exchange arising from transient interactions with either the TMH or the headgroup region of the micelle. Since the APH is not required for the structural integrity and activity of the tetrameric ion channel,[60] and only a small TMH−APH interface is present in the solid state structure,[35] it seems unlikely that strong interactions between the TMH and APH occur. In contrast, the observations that APH resonances in micelles were not strongly affected by the addition of a water-soluble paramagnetic nuclei and that relatively small chemical shift changes were observed in the APH upon addition of DPPC suggest that the APH interacts with phosphocholine headgroups in both micelles and bicelles but that variability in these interactions in micelles gave rise to the observed conformational exchange. The observation of a large increase in the quality of the fits of bicelle RDC data to the static structures supports this hypothesis: flexibility in the TMH−APH linker residues that leads to fluctuations in the relative orientation of the TMH and APH is expected to degrade the fit quality. The dynamic nature of the DHPC micelle[61] may permit large-scale deformations of the micelle surface to which the APH remains associated. That the bicelle RDCs fit

comparably well to either the solid state or the solution NMR structure is unsurprising given the similarity in the angles between the TMH and APH in the two structures.

Residues within the N-terminal half of the TMH also exhibited relatively large chemical shift changes. Tight intersubunit packing in this region of the TMH has been observed in most structures of M2, suggesting that this region would be sensitive to changes in subunit alignment within the tetramer. The RDCs combined with the chemical shift changes observed in residues near Gly34 suggest that a change in the relative orientation of the N-terminal and C-terminal segments of the TMH occurs upon addition of lipids. Such changes in the TMH kink at Gly34 have been observed in studies of a TMH-only construct of Udorn M2 in lipid bilayers,[58] in which membrane depth was adjusted by changing the lipid composition. Interestingly, the largest changes in the TMH occur near the high affinity amino-adamantyl drug binding site, binding of which is known to be dependent on both the solubilizing agent and the presence of the APH.[58,59]

In conclusion, the results presented here suggest that solubilization of swM2 into bicelles results in an increased ordering of the TMH−APH linker resulting in a more fixed orientation between the TMH and APH. Furthermore, we show that the swM2 construct, which is based on currently circulating strains of influenza, is particularly amenable to high resolution solution NMR studies in the presence of lipids. This study will enable further work to be carried out elucidating the molecular details of M2 interactions with lipids.

■ ASSOCIATED CONTENT

Supporting Information

Figures showing an alignment of selected M2 sequences, chemical cross-linking results, a spectral overlay of swM2 in bicelles of different q values, a 2D NOESY spectrum showing NOEs to lipid, a secondary chemical shift analysis and RCI plot for swM2 in micelles and bicelles, NMR spectra of the Udorn variant in micelles and bicelles, NMR spectra of swM2 in bicelles containing different lipids, and TRACT relaxation data. This material is available free of charge via the Internet at http://pubs.acs.org.

■ AUTHOR INFORMATION

Corresponding Author

*E-mail: jason.schnell@bioch.ox.ac.uk. Phone: +44 01865 613350.

Present Address

[†]J.A.: D. E. Shaw Research, 120 W. 45th St., 39th Fl., New York, NY 10036, USA.

Funding

The research was funded by the MRC (Grant G0901012). J.A. was funded by the Osk. Huttunen Foundation (Helsinki, Finland).

Notes

The authors declare no competing financial interest.

■ ACKNOWLEDGMENTS

Donghan Lee is thanked for providing the TRACT pulse sequence. Nick Soffe and Jonathan Boyd are acknowledged for assistance with NMR data acquisition.

■ ABBREVIATIONS

3D, three-dimensional; APH, amphipathic helix; DHPC, 1,2-dihexanoyl-*sn*-glycero-3-phosphocholine; DOPC, 1,2-dioleoyl-*sn*-glycero-3-phosphocholine; DOPE, 1,2-dioleoyl-*sn*-glycero-3-phosphoethanolamine; DPPC, 1,2-dipalmitoyl-*sn*-glycero-3-phosphocholine; HEPES, 4-(2-hydroxyethyl)piperazine-1-ethanesulfonic acid; HFIP, hexafluoroisopropanol; HPLC, high-performance liquid chromatography; M2, matrix protein 2; NMR, nuclear magnetic resonance; R_1, longitudinal relaxation rate; R_2, transverse relaxation rate; RDC, residual dipolar coupling; TFA, trifluoroacetic acid; TMH, transmembrane helix

■ REFERENCES

(1) Hay, A. J., Wolstenholme, A. J., Skehel, J. J., and Smith, M. H. (1985) The molecular basis of the specific anti-influenza action of amantadine. *EMBO J. 4*, 3021−3024.

(2) Pinto, L. H., Holsinger, L. J., and Lamb, R. A. (1992) Influenza virus M2 protein has ion channel activity. *Cell 69*, 517−528.

(3) Lamb, R. A., Zebedee, S. L., and Richardson, C. D. (1985) Influenza virus M2 protein is an integral membrane protein expressed on the infected-cell surface. *Cell 40*, 627−633.

(4) Helenius, A. (1992) Unpacking the incoming influenza virus. *Cell 69*, 577−578.

(5) Steinhauer, D. A., Wharton, S. A., Skehel, J. J., Wiley, D. C., and Hay, A. J. (1991) Amantadine selection of a mutant influenza virus containing an acid-stable hemagglutinin glycoprotein: Evidence for virus-specific regulation of the pH of glycoprotein transport vesicles. *Proc. Natl. Acad. Sci. U. S. A. 88*, 11525−11529.

(6) Wang, J., Qiu, J. X., Soto, C., and DeGrado, W. F. (2011) Structural and dynamic mechanisms for the function and inhibition of the M2 proton channel from influenza A virus. *Curr. Opin. Struct. Biol. 21*, 68−80.

(7) Pinto, L. H., and Lamb, R. A. (2006) Influenza virus proton channels. *Photochem. Photobiol. Sci. 5*, 629−632.

(8) Cross, T. A., Dong, H., Sharma, M., Busath, D. D., and Zhou, H. X. (2012) M2 protein from influenza A: From multiple structures to biophysical and functional insights. *Curr. Opin. Virol. 2*, 128−133.

(9) Bright, R. A., Shay, D. K., Shu, B., Cox, N. J., and Klimov, A. I. (2006) Adamantane resistance among influenza A viruses isolated early during the 2005−2006 influenza season in the United States. *JAMA, J. Am. Med. Assoc. 295*, 891−894.

(10) Govorkova, E. A., Baranovich, T., Seiler, P., Armstrong, J., Burnham, A., Guan, Y., Peiris, M., Webby, R. J., and Webster, R. G. (2013) Antiviral resistance among highly pathogenic influenza A (H5N1) viruses isolated worldwide in 2002−2012 shows need for continued monitoring. *Antiviral Res. 98*, 297−304.

(11) Chen, Y., Liang, W., Yang, S., Wu, N., Gao, H., Sheng, J., Yao, H., Wo, J., Fang, Q., Cui, D., Li, Y., Yao, X., Zhang, Y., Wu, H., Zheng, S., Diao, H., Xia, S., Chan, K. H., Tsoi, H. W., Teng, J. L., Song, W., Wang, P., Lau, S. Y., Zheng, M., Chan, J. F., To, K. K., Chen, H., Li, L., and Yuen, K. Y. (2013) Human infections with the emerging avian influenza A H7N9 virus from wet market poultry: clinical analysis and characterisation of viral genome. *Lancet 381*, 1916−1925.

(12) Astrahan, P., Flitman-Tene, R., Bennett, E. R., Krugliak, M., Gilon, C., and Arkin, I. T. (2011) Quantitative analysis of influenza M2 channel blockers. *Biochim. Biophys. Acta 1808*, 394−398.

(13) Rossman, J. S., Jing, X., Leser, G. P., and Lamb, R. A. (2010) Influenza virus M2 protein mediates ESCRT-independent membrane scission. *Cell 142*, 902−913.

(14) Schroeder, C., Heider, H., Moncke-Buchner, E., and Lin, T. I. (2005) The influenza virus ion channel and maturation cofactor M2 is a cholesterol-binding protein. *Eur. Biophys. J. 34*, 52−66.

(15) McCown, M. F., and Pekosz, A. (2005) The influenza A virus M2 cytoplasmic tail is required for infectious virus production and efficient genome packaging. *J. Virol. 79*, 3595−3605.

(16) Chen, B. J., Leser, G. P., Jackson, D., and Lamb, R. A. (2008) The influenza virus M2 protein cytoplasmic tail interacts with the M1

protein and influences virus assembly at the site of virus budding. *J. Virol. 82*, 10059−10070.
(17) Thaa, B., Levental, I., Herrmann, A., and Veit, M. (2011) Intrinsic membrane association of the cytoplasmic tail of influenza virus M2 protein and lateral membrane sorting regulated by cholesterol binding and palmitoylation. *Biochem. J. 437*, 389−397.
(18) Rossman, J. S., Jing, X., Leser, G. P., Balannik, V., Pinto, L. H., and Lamb, R. A. (2010) Influenza virus M2 ion channel protein is necessary for filamentous virion formation. *J. Virol. 84*, 5078−5088.
(19) Roberts, K. L., Leser, G. P., Ma, C., and Lamb, R. A. (2013) The amphipathic helix of influenza A virus M2 protein is required for filamentous bud formation and scission of filamentous and spherical particles. *J. Virol. 87*, 9973−9982.
(20) Cross, T. A., Sharma, M., Yi, M., and Zhou, H. X. (2011) Influence of solubilizing environments on membrane protein structures. *Trends Biochem. Sci. 36*, 117−125.
(21) Pielak, R. M., Oxenoid, K., and Chou, J. J. (2011) Structural investigation of rimantadine inhibition of the AM2-BM2 chimera channel of influenza viruses. *Structure 19*, 1655−1663.
(22) Wang, J., Wu, Y., Ma, C., Fiorin, G., Pinto, L. H., Lamb, R. A., Klein, M. L., and Degrado, W. F. (2013) Structure and inhibition of the drug-resistant S31N mutant of the M2 ion channel of influenza A virus. *Proc. Natl. Acad. Sci. U. S. A. 110*, 1315−1320.
(23) Schnell, J. R., and Chou, J. J. (2008) Structure and mechanism of the M2 proton channel of influenza A virus. *Nature 451*, 591−595.
(24) Chou, J. J., Kaufman, J. D., Stahl, S. J., Wingfield, P. T., and Bax, A. (2002) Micelle-induced curvature in a water-insoluble HIV-1 Env peptide revealed by NMR dipolar coupling measurement in stretched polyacrylamide gel. *J. Am. Chem. Soc. 124*, 2450−2451.
(25) Andersson, A., and Maler, L. (2005) Magnetic resonance investigations of lipid motion in isotropic bicelles. *Langmuir 21*, 7702−7709.
(26) Luchette, P. A., Vetman, T. N., Prosser, R. S., Hancock, R. E., Nieh, M. P., Glinka, C. J., Krueger, S., and Katsaras, J. (2001) Morphology of fast-tumbling bicelles: a small angle neutron scattering and NMR study. *Biochim. Biophys. Acta 1513*, 83−94.
(27) Glover, K. J., Whiles, J. A., Wu, G., Yu, N., Deems, R., Struppe, J. O., Stark, R. E., Komives, E. A., and Vold, R. R. (2001) Structural evaluation of phospholipid bicelles for solution-state studies of membrane-associated biomolecules. *Biophys. J. 81*, 2163−2171.
(28) Poget, S. F., Cahill, S. M., and Girvin, M. E. (2007) Isotropic bicelles stabilize the functional form of a small multidrug-resistance pump for NMR structural studies. *J. Am. Chem. Soc. 129*, 2432−2433.
(29) Morrison, E. A., DeKoster, G. T., Dutta, S., Vafabakhsh, R., Clarkson, M. W., Bahl, A., Kern, D., Ha, T., and Henzler-Wildman, K. A. (2011) Antiparallel EmrE exports drugs by exchanging between asymmetric structures. *Nature 481*, 45−50.
(30) Bocharov, E. V., Pustovalova, Y. E., Pavlov, K. V., Volynsky, P. E., Goncharuk, M. V., Ermolyuk, Y. S., Karpunin, D. V., Schulga, A. A., Kirpichnikov, M. P., Efremov, R. G., Maslennikov, I. V., and Arseniev, A. S. (2007) Unique dimeric structure of BNip3 transmembrane domain suggests membrane permeabilization as a cell death trigger. *J. Biol. Chem. 282*, 16256−16266.
(31) Lau, T. L., Kim, C., Ginsberg, M. H., and Ulmer, T. S. (2009) The structure of the integrin alphaIIbbeta3 transmembrane complex explains integrin transmembrane signalling. *EMBO J. 28*, 1351−1361.
(32) Bocharov, E. V., Mayzel, M. L., Volynsky, P. E., Goncharuk, M. V., Ermolyuk, Y. S., Schulga, A. A., Artemenko, E. O., Efremov, R. G., and Arseniev, A. S. (2008) Spatial structure and pH-dependent conformational diversity of dimeric transmembrane domain of the receptor tyrosine kinase EphA1. *J. Biol. Chem. 283*, 29385−29395.
(33) Bocharov, E. V., Mayzel, M. L., Volynsky, P. E., Mineev, K. S., Tkach, E. N., Ermolyuk, Y. S., Schulga, A. A., Efremov, R. G., and Arseniev, A. S. (2010) Left-handed dimer of EphA2 transmembrane domain: Helix packing diversity among receptor tyrosine kinases. *Biophys. J. 98*, 881−889.
(34) Endres, N. F., Das, R., Smith, A. W., Arkhipov, A., Kovacs, E., Huang, Y., Pelton, J. G., Shan, Y., Shaw, D. E., Wemmer, D. E., Groves, J. T., and Kuriyan, J. (2013) Conformational coupling across the plasma membrane in activation of the EGF receptor. *Cell 152*, 543−556.
(35) Sharma, M., Yi, M., Dong, H., Qin, H., Peterson, E., Busath, D. D., Zhou, H. X., and Cross, T. A. (2010) Insight into the mechanism of the influenza A proton channel from a structure in a lipid bilayer. *Science 330*, 509−512.
(36) Claridge, J. K., and Schnell, J. R. (2012) Bacterial production and solution NMR studies of a viral membrane ion channel. *Methods Mol. Biol. 831*, 165−179.
(37) Delaglio, F., Grzesiek, S., Vuister, G. W., Zhu, G., Pfeifer, J., and Bax, A. (1995) NMRPipe: A multidimensional spectral processing system based on UNIX pipes. *J. Biomol. NMR 6*, 277−293.
(38) Keller, R. (2004) Optimizing the process of nuclear magnetic resonance spectrum analysis and computer aided resonance assignment, p 149, Swiss Federal Institute of Technology Zurich, Zurich.
(39) Vranken, W. F., Boucher, W., Stevens, T. J., Fogh, R. H., Pajon, A., Llinas, M., Ulrich, E. L., Markley, J. L., Ionides, J., and Laue, E. D. (2005) The CCPN data model for NMR spectroscopy: development of a software pipeline. *Proteins 59*, 687−696.
(40) Farrow, N. A., Zhang, O., Forman-Kay, J. D., and Kay, L. E. (1995) Comparison of the backbone dynamics of a folded and an unfolded SH3 domain existing in equilibrium in aqueous buffer. *Biochemistry 34*, 868−878.
(41) Hwang, T. L., van Zijl, P. C., and Mori, S. (1998) Accurate quantitation of water-amide proton exchange rates using the phase-modulated CLEAN chemical EXchange (CLEANEX-PM) approach with a Fast-HSQC (FHSQC) detection scheme. *J. Biomol. NMR 11*, 221−226.
(42) Lee, D., Hilty, C., Wider, G., and Wüthrich, K. (2006) Effective rotational correlation times of proteins from NMR relaxation interference. *J. Magn. Reson. 178*, 72−76.
(43) Chou, J. J., Gaemers, S., Howder, B., Louis, J. M., and Bax, A. (2001) A simple apparatus for generating stretched polyacrylamide gels, yielding uniform alignment of proteins and detergent micelles. *J. Biomol. NMR 21*, 377−382.
(44) Tycko, R., Blanco, F. J., and Ishii, Y. (2000) Alignment of biopolymers in strained gels: A new way to create detectable dipole−dipole couplings in high-resolution biomolecular NMR. *J. Am. Chem. Soc. 122*, 9340−9341.
(45) Andersson, A., Biverstahl, H., Nordin, J., Danielsson, J., Lindahl, E., and Maler, L. (2007) The membrane-induced structure of melittin is correlated with the fluidity of the lipids. *Biochim. Biophys. Acta 1768*, 115−121.
(46) Andersson, A., Danielsson, J., Graslund, A., and Maler, L. (2007) Kinetic models for peptide-induced leakage from vesicles and cells. *Eur. Biophys. J. 36*, 621−635.
(47) Li, H., Yao, Z., Degenhardt, B., Teper, G., and Papadopoulos, V. (2001) Cholesterol binding at the cholesterol recognition/ interaction amino acid consensus (CRAC) of the peripheral-type benzodiazepine receptor and inhibition of steroidogenesis by an HIV TAT-CRAC peptide. *Proc. Natl. Acad. Sci. U. S. A. 98*, 1267−1272.
(48) Sugrue, R. J., and Hay, A. J. (1991) Structural characteristics of the M2 protein of influenza A viruses: Evidence that it forms a tetrameric channel. *Virology 180*, 617−624.
(49) Holsinger, L. J., and Lamb, R. A. (1991) Influenza virus M2 integral membrane protein is a homotetramer stabilized by formation of disulfide bonds. *Virology 183*, 32−43.
(50) Rath, A., Glibowicka, M., Nadeau, V. G., Chen, G., and Deber, C. M. (2009) Detergent binding explains anomalous SDS-PAGE migration of membrane proteins. *Proc. Natl. Acad. Sci. U. S. A. 106*, 1760−1765.
(51) Rath, A., and Deber, C. M. (2013) Correction factors for membrane protein molecular weight readouts on sodium dodecyl sulfate-polyacrylamide gel electrophoresis. *Anal. Biochem. 434*, 67−72.
(52) Pielak, R. M., Schnell, J. R., and Chou, J. J. (2009) Mechanism of drug inhibition and drug resistance of influenza A M2 channel. *Proc. Natl. Acad. Sci. U. S. A. 106*, 7379−7384.

(53) Shen, Y., Delaglio, F., Cornilescu, G., and Bax, A. (2009) TALOS+: a hybrid method for predicting protein backbone torsion angles from NMR chemical shifts. *J. Biomol. NMR 44*, 213−223.
(54) Berjanskii, M. V., and Wishart, D. S. (2005) A simple method to predict protein flexibility using secondary chemical shifts. *J. Am. Chem. Soc. 127*, 14970−14971.
(55) Kay, L. E., Torchia, D. A., and Bax, A. (1989) Backbone dynamics of proteins as studied by 15N inverse detected heteronuclear NMR spectroscopy: Application to staphylococcal nuclease. *Biochemistry 28*, 8972−8979.
(56) Kneller, J. M., Lu, M., and Bracken, C. (2002) An effective method for the discrimination of motional anisotropy and chemical exchange. *J. Am. Chem. Soc. 124*, 1852−1853.
(57) Nguyen, P. A., Soto, C. S., Polishchuk, A., Caputo, G. A., Tatko, C. D., Ma, C., Ohigashi, Y., Pinto, L. H., DeGrado, W. F., and Howard, K. P. (2008) pH-induced conformational change of the influenza M2 protein C-terminal domain. *Biochemistry 47*, 9934−9936.
(58) Hu, F., Luo, W., Cady, S. D., and Hong, M. (2011) Conformational plasticity of the influenza A M2 transmembrane helix in lipid bilayers under varying pH, drug binding, and membrane thickness. *Biochim. Biophys. Acta 1808*, 415−423.
(59) Cady, S., Wang, T., and Hong, M. (2011) Membrane-dependent effects of a cytoplasmic helix on the structure and drug binding of the influenza virus M2 protein. *J. Am. Chem. Soc. 133*, 11572−11579.
(60) Ma, C., Polishchuk, A. L., Ohigashi, Y., Stouffer, A. L., Schon, A., Magavern, E., Jing, X., Lear, J. D., Freire, E., Lamb, R. A., DeGrado, W. F., and Pinto, L. H. (2009) Identification of the functional core of the influenza A virus A/M2 proton-selective ion channel. *Proc. Natl. Acad. Sci. U. S. A. 106*, 12283−12288.
(61) Rouse, S. L. The Influence of Environment: Simulations of the Influenza BM2 Proton Channel, PhD dissertation, Department of Biochemistry, University of Oxford, Oxford, UK.